

Optical properties of twinning superlattices in diamond-type and zinc-blende-type semiconductors

Z. Ikonc, G. P. Srivastava, and J. C. Inkson

Department of Physics, Exeter University, Stocker Road, Exeter, EX4 4QL, United Kingdom

(Received 27 April 1995)

The optical properties (interband and intraband absorption) of a recently proposed structure—twinning superlattices—in diamond-type and zinc-blende-type semiconductors are calculated and discussed. The conduction-band intraband absorption is found to be rather weak, but the intraband absorption between the valence-band states has rather high values. Direct (phononless) interband absorption in twinning superlattices based on indirect gap semiconductors like germanium is also found to be allowed.

I. INTRODUCTION

Traditionally, two types of superlattices have been grown, based on periodic modulation of either the material composition or doping. Formation of the miniband spectrum in both types is usually interpreted as a consequence of a periodic potential experienced by electrons. Alternatively, miniband formation may be viewed as due to periodic electron scattering in such structures. We have recently proposed another type of superlattice—the twinning superlattice.¹ Structurally, it is a periodic array of twinning boundaries in a semiconductor that is otherwise homogeneous; i.e., no modulation of its composition or doping is involved. Thus the twinning superlattice comprises periodic change of orientation of the underlying crystal, or, to give a more microscopic view, of an atomic stacking sequence along the superlattice axis. For twinning superlattices based on zinc-blende-type semiconductors, there are two possible crystal orientations, one rotated by 180° with respect to the other about the [111] axis, if the interface is to remain perfect. The simplest form of such a superlattice would therefore include n and m atomic bilayers of oppositely oriented material per period, constituting an (n, m) twinning superlattice. Certainly, more complicated structures of a period, e.g., (n, m, p, q) , may also exist. We also note that, related to them, polytypic superlattices^{2,3} may be interpreted as a special class of twinning superlattices in diamond/zinc-blende crystals, but the latter are more general and could also be envisaged in various other crystal systems, provided they allow for twinning.⁴

Twinning, as well as more complex structures derived from it (i.e., stacking faults), are commonly found in both natural minerals and artificially grown crystals (in the latter case they are usually considered as undesired defects). Although not much research effort has been put into fabrication of high-quality structures of these types, some promising progress has been made. In particular, a high-quality, possibly large area, single twin boundary in silicon has been grown by depositing a submonolayer of boron during the molecular-beam-epitaxy growth.⁵ Another interesting finding is reported in Refs. 6 and 7, where free-standing GaAs quantum wire whiskers were found to have the structure of somewhat irregular twin-

ning superlattices, their periods being quite small, in the nanometer range, just as the wire diameters themselves. While single twins are commonly found in more macroscopic whiskers,⁸ small diameter wires grown in Refs. 6 and 7 seem to promote multiple twinning. Also interesting is the occurrence of a large number of twinning lamellae in bulk zinc-blende CdTe when alloyed with (rocksalt) MnTe. With individual lamellae thickness in the micron range no quantization effects are expected here, but the structure may be of use in nonlinear optics.⁹ In view of all these reports, fabrication of a twinning superlattice structure may seem quite feasible in the near future.

A detailed account of the electronic properties of twinning superlattices is given in our previous paper.¹⁰ Here we shall only briefly recapitulate their essentials relevant for optical properties. To understand how the electron scattering comes about despite lack of modulation of the potential, the effective mass, or the lattice type, we note that both the in-plane structure of the wave functions and the dispersion along the [111] direction are generally not invariant under the 180° rotation. In terms of electron wave-function propagation, therefore, a twin behaves as a junction of two essentially *different* materials. To give a more detailed description, we recall that the Γ and two out of the eight L bulk Brillouin zone points are projected onto $\bar{\Gamma}$, while all the six X and six “tilted” L points (in pairs, one of each kind) project onto six \bar{M} points of the hexagonal interface Brillouin zone (shown, e.g., in Fig. 1 of Ref. 10). Therefore, $\bar{\Gamma}$ and \bar{M} are the most important \mathbf{k}_{\parallel} points of the interface Brillouin zone to govern the electronic and optical properties of twinning superlattices. The symmetry mismatch gives rise to interface mixing/coupling of the corresponding bulk crystal states which project onto these points of the interface Brillouin zone. The magnitude of the effect is much larger at \bar{M} than at the $\bar{\Gamma}$ point. Also, mixing of different bulk states is enhanced if their energies are close to each other (for instance, it is much stronger in Ge- than in Si-based twinning superlattices). In any case, the strength of the resulting scattering is high enough to generate a prominent miniband structure of twinning superlattices.

In this paper we calculate optical properties of twinning superlattices, i.e., intersubband and interband ab-

sorption arising from single-photon direct (phononless) transitions. With the miniband structure appearing in both the conduction and valence bands, intersubband transitions within each band should be possible, just as they are in conventional superlattices. Furthermore, interband transitions, involving minibands of the conduction and valence bands, should also be possible as direct transitions, provided that the relevant miniband extrema occur at the same point of the superlattice Brillouin zone. Since the valence-band states are at its center, the conduction-band states that arrive there by folding would become optically active even in superlattices based on indirect-gap semiconductors.

II. THE METHOD

The method used in our calculations is an empirical pseudopotential-based layer method.¹¹ It uses the bulk band-structure data to find properties of more complex (micro)structures. Basically, we first calculate the complex band structure and eigenfunctions of both the propagating and evanescent states of the two bulk semiconductors on either side of the interface. The in-plane (\mathbf{g}_{\parallel}) Fourier components of the eigenfunctions are then matched at the interface(s) and then the functions propagated along the layers. The wave-function propagation and matching is performed using the S -matrix approach, which guarantees high stability against the evanescent states.¹¹ Once the S matrix of the superlattice period d is found, it is recast into the transfer (T) matrix, and the Bloch theorem applied,¹² as $T\Psi = \exp(ik_z d)\Psi$, where k_z is the wave vector in the superlattice growth direction. Thus, this method does not belong to the class of supercell methods. All the results obtained within it are subject to interpretation via the bulk band-structure concepts. Yet, along with the advantage of simplicity, such a calculation does reveal all the band-structure-related properties of twinning superlattices arising from band mixing and bulk Brillouin zone folding. Furthermore, in case of single twinning boundaries and stacking faults, the results obtained from this method show good quantitative comparison to those obtained by more elaborate self-consistent calculations.^{13,14}

A point to note here, of relevance for calculation of optical properties, is that different superlattice state wave functions, calculated as described above, are not required to be orthogonal because all are right eigenvectors of a complex non-Hermitian eigenvalue problem. In fact they should be orthogonal (as is also obvious for physical reasons), because of the special structure of the T matrix, but in practice the numerical errors present will induce some amount of nonorthogonality. This is different from what one obtains within the supercell approach. Because the wave functions there are found as eigenvectors of the supercell Hamiltonian, they are forced (by the diagonalization routine) to be orthogonal in spite of any numerical errors present therein. The degree of orthogonality of wave functions encountered in our calculations was generally quite good, overlap between different states usually amounted to well below 1%, and only occasionally went somewhat out of this range. However, to avoid spurious

results the pairs of wave functions to be used in the transition matrix element calculation were first Lowdin orthogonalized. This property ensures that the matrix elements between two states, say 1 and 2, i.e., p_{12} and p_{21} , are exactly equal.

In order to calculate the optical absorption in twinning superlattices we tabulate for all the relevant minibands their dispersion $E(\mathbf{k}_{\parallel}, k_z)$. We are interested here in absorption for only a limited range of photon energies, from about the threshold value for any particular type of absorption to a few hundred meV above. This limits the range of states within the superlattice Brillouin zone to be considered. While k_z spans the whole superlattice Brillouin zone, because the miniband widths are not very large, the range of \mathbf{k}_{\parallel} values of interest is much smaller, they typically occupy areas in the interface Brillouin zone, positioned at \bar{M} and $\bar{\Gamma}$ points, which are two orders of magnitude smaller than the interface Brillouin zone itself. Within these restricted volumes of the superlattice Brillouin zone energies for each miniband and the transition matrix elements are tabulated in 80–150 points of the \mathbf{k} space, and in calculating the absorption interpolation is used for \mathbf{k} points in between this coarse grid. While the number of grid points used in the calculation of matrix elements and energies may seem large as compared to what is necessary in conventional superlattices, this is not so in twinning superlattices: due to the \mathbf{k} -dependent band mixing effects, the matrix elements tend to vary by more than an order of magnitude, and for the same reason the separation of miniband energies, and hence the joint density of states, varies significantly as \mathbf{k}_{\parallel} varies.

The absorption coefficient is calculated from

$$\alpha = \frac{e^2}{\pi^2 m_0^2 n \epsilon_0 \omega c} \times \sum_{i,f} \int \int \int |p_{if}|^2 f_{if}(E_f) \delta(E_f - E_i - \hbar\omega) d^3k ,$$

where m_0 and e are the free electron mass and charge, c speed of light, n the refraction index, ϵ_0 the dielectric permittivity of vacuum, $\hbar\omega$ the photon energy, p_{if} the light polarization dependent momentum matrix element between the states having the same \mathbf{k} vector in minibands i and f , with energies E_i and E_f , f_{if} is the difference of Fermi-Dirac functions for these two states, which depends on the Fermi level E_F . In real calculations the δ function is replaced by a Lorentzian of a suitable half-width γ , for both the computational convenience and modeling the linewidth broadening effects like electron scattering. For this latter reason we have chosen $\gamma = 5$ meV, a typical value used in calculations of optical properties of semiconductor quantum wells.

In the case of interband absorption no doping of the superlattice needs to be assumed, because the valence band is completely filled with electrons. In the case of intersubband absorption, the superlattice has to be n doped (p doped) for transitions between the conduction-band (valence-band) states to occur, and the doping level has to be related to the Fermi energy E_F .

III. RESULTS AND DISCUSSION

Numerical calculations of the miniband structure have been performed using the empirical pseudopotential form factors from Refs. 15, 16, and 17 for Si, Ge, and GaAs, respectively. In the pseudopotential layer method we used a total of 19 in-plane Fourier components (g_{\parallel} values) in interface matching, corresponding to a total of 59 three-dimensional reciprocal lattice vectors, up to and including the (222) star. Intersubband transitions in the conduction band are calculated without the spin-orbit interaction included. There is a rather slight influence of the spin-orbit interaction on conduction-band states in twinning superlattices. The most important one is the removal of zero energy gaps between pairs of adjacent minibands¹⁰ that exist for any k_{\parallel} value without, and remain only at the $\bar{\Gamma}$ point with the spin-orbit interaction. However, the amount of the spin-orbit-induced splitting of zero energy gaps is not very large, typically a couple of meV close to the \bar{M} point, and an order of magnitude less than that close to the $\bar{\Gamma}$ point. This is much less than other features of the electronic structures (changes in miniband and minigap widths as k_{\parallel} varies), and this splitting can hardly influence the absorption line shape, except at extremely small photon energies. There is also no significant influence of the spin-orbit coupling on matrix elements themselves (this was checked for). Intersubband transitions in the valence band, and interband transitions, however, were treated with the spin-orbit interaction included, because of its essential influence on valence-band wave functions.

The absorption coefficient was calculated for intersubband transitions (within the conduction and valence bands) in Si- and Ge-based superlattices, and for interband transitions in Ge- and GaAs-based superlattices. Cases of light polarization both along the superlattice axis (z), or in-plane (x, y) were considered. In the latter case the absorption arising from transitions between minibands at any one of equivalent \bar{M} points is not isotropic in the x - y plane, but becomes isotropic when contributions from all six \bar{M} points are added together.

A. Intersubband transitions

The miniband structure within the conduction band for some of the superlattices considered here is given in detail in our previous paper.¹⁰ However, all these data are given here in the compressed form as insets in the figures displaying the calculated absorption. With the miniband structure calculated we first find the Fermi level (entering the absorption coefficient) so as to correspond to a desired doping level, i.e., electron or hole density and temperature. In all the calculations presented below the doping (n or p type) is assumed to be 10^{17} cm^{-3} , and temperature is set at $T = 77$ or 300 K. At this doping level the Fermi energy is below the lowest allowed miniband energy available, and it remains so until the doping reaches $(3-5) \times 10^{17}$ cm^{-3} , or even larger values at 300 K. This means that, as doping level varies, the state filling follows in a proportional, not saturating, manner, and the absorption profiles should scale linearly with the

doping level. In Si-based superlattices the only important minibands are those at the \bar{M} point. It is found that only the first miniband is populated at 77 K, and at 300 K a small fraction ($\leq 10\%$) of the electron density goes into the second miniband. In Ge-based superlattices the situation is more complicated. Here we have two groups of minibands, at \bar{M} and $\bar{\Gamma}$ points, both of which stem from L valleys and therefore have energies in the same range. At the $\bar{\Gamma}$ point there is an interface state and the lowest miniband it generates is somewhat below the bulk conduction-band edge. There is no interface state at the exact \bar{M} point (and the lowest miniband edge there is above the conduction-band edge), but it appears when k_{\parallel} moves slightly inwards of the interface Brillouin zone (by approximately 13% of the $\bar{\Gamma}$ - \bar{M} line length), and the lowest miniband edge here is lower than at the exact \bar{M} point, although it is still slightly higher than the one at the $\bar{\Gamma}$ point. Due to a small transverse and large longitudinal effective mass of the L valley, the density of states for $\bar{\Gamma}$ minibands is considerably lower than that for \bar{M} minibands. It happens then that at 77 K almost all of the electrons reside in the lowest $\bar{\Gamma}$ miniband, but at 300 K they take advantage of a larger density of states offered by \bar{M} minibands, and about 70% of the electron density goes here. The increase of temperature thus transforms Ge-based twinning superlattice from a quasi-direct-gap into an indirect-gap material.

The calculated absorption profiles arising from intersubband transitions within the conduction band for a few twinning superlattices based on Si and Ge are given in Figs. 1(a)–(d) and Figs. 2(a) and 2(b), respectively. The insets in them display the miniband structure at point(s) of the interface Brillouin zone where miniband energies are lowest. In both Si- and Ge-based superlattices this is at a point slightly away from \bar{M} along the $\bar{\Gamma}$ - \bar{M} line [at $k_{\parallel} = 0.87k_{\parallel}(\bar{M})$], and in Ge at the $\bar{\Gamma}$ point as well. Also denoted along the absorption lines are the transitions responsible for various features in them.

When compared with values of optical absorption obtainable in conventional quantum wells or superlattices, including those based on indirect-band-gap materials,¹⁸ where absorption coefficients of the order of 10^3 cm^{-1} are typical for electron density as used here, the intersubband absorption within the conduction band in twinning superlattices is clearly rather low, which is mainly due to the comparatively low values of transition matrix elements.

An intuitive understanding of why this is so may be obtained by making a digression to the nearly-free-electron picture of miniband formation in superlattices. Considering first a fictitious superlattice of period n , “made” by taking n unit cells of a homogeneous bulk crystal to constitute one period (supercell) of such a superlattice. One knows that the “miniband” dispersion here is just the bulk dispersion folded in the shrunken first Brillouin zone of the fictitious superlattice, and the wave functions in the two cases are identical except for the difference in interpretation of what is the periodic part of the Bloch function and what is its phase. That vertical transitions between different “minibands” in this case are forbidden follows, within the supercell picture, not because they *would* be skewed (not \mathbf{k} conserving) in the unfolded repre-

sentation, but rather because the transition matrix element calculated within the supercell is equal to zero. This is due to cancellation of contributions from volumes of single unit cells constituting a supercell, brought about by assigning part of the bulk Bloch function phase to the supercell periodic part of the Bloch function. Now, consider a real but very "weak" superlattice, such that the introduced periodic modulation of a potential or structure composition opens small finite gaps at the superlattice Brillouin zone edges, separating comparatively broad allowed minibands. The nearly free electron model indicates that the superlattice wave functions are not very different from the folded bulk wave functions, except for states close to miniband gaps. While the transition matrix elements between various minibands will now generally have nonzero values, they cannot be large, since nothing much has changed physically. The situation in "weak" superlattices is thus quite different from that in a system of weakly coupled multiple quantum wells, known to offer substantial values of transition matrix elements

(e.g., the dipole matrix elements of the order of $\frac{1}{5}$ of well dimensions are usual, and enable large absorption, as stated above). The expectation that similar values should be obtained in any superlattice is quite misleading: what matters, somewhat vaguely speaking, is how much the wave functions of superlattice states (provided they belong to the same band) deviate from pure folded bulk wave functions.

The rather broad miniband structure of various twinning superlattices considered here (insets in Figs. 1 and 2) is much more similar to the weak superlattice case, than to almost dispersionless states in multiple quantum wells, and the above discussion should thus be applicable. Indeed, in Si-based superlattices where the states in the vicinity of the \bar{M} point are important, the transition matrix elements between such states (and the absorption) are not large because X_1 , X_3 , and L states in Si are widely spaced and do not allow for large mixing. Additionally, by comparing the results for $(n, m \neq n)$ and (n, n) superlattices [Figs. 1(a)–1(d)] one can see that the former

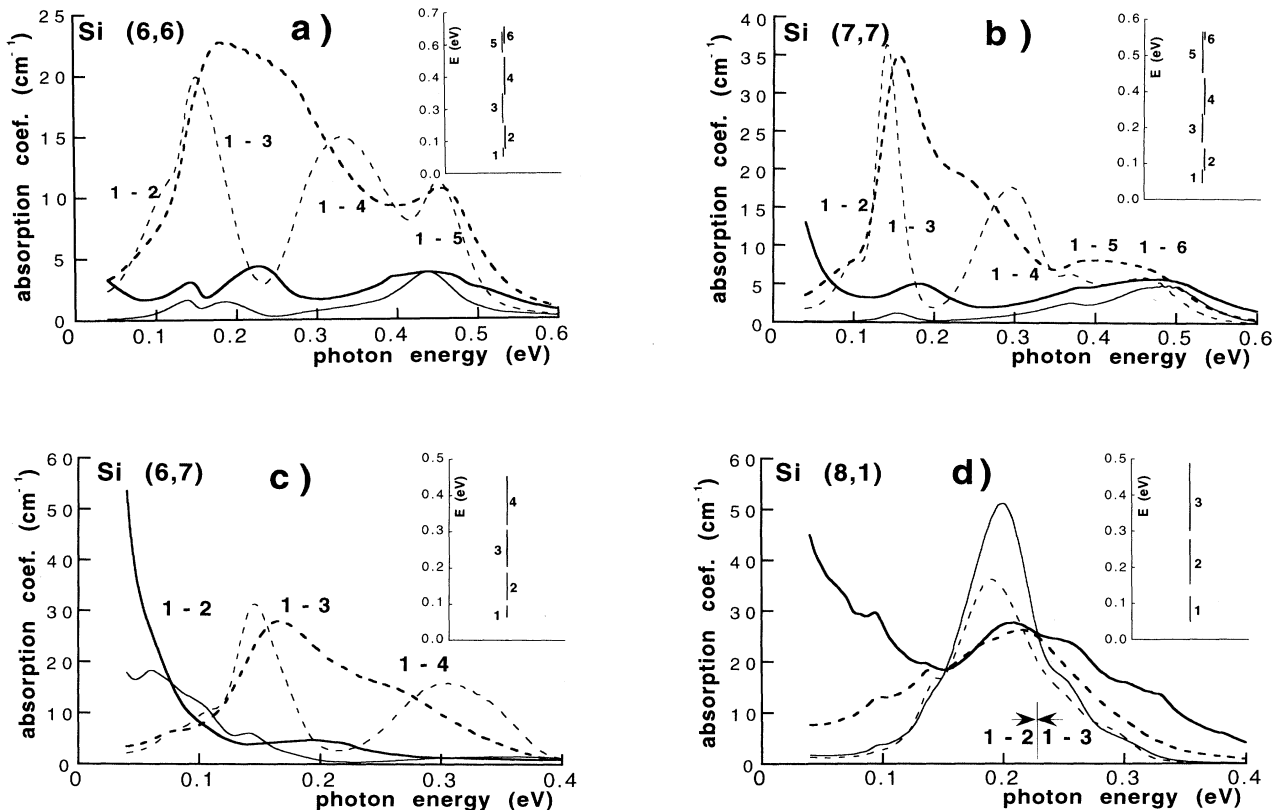


FIG. 1. The absorption coefficient arising from intersubband transitions within the conduction band in Si-based twinning superlattices: (a) Si (6,6), (b) Si(7,7), (c) Si(6,7), and (d) Si(8,1). The electron density is $n = 10^{17} \text{ cm}^{-3}$. Thick lines correspond to the temperature $T = 300 \text{ K}$, and thin lines to $T = 77 \text{ K}$. The solid lines are for light polarized along the z axis, and the dashed lines for the in-plane (x, y) polarization. The insets in all the figures display the energy range of the minibands in the corresponding superlattices at the point close to the \bar{M} point of the interface Brillouin zone, where these energies are lowest (energies are measured from the conduction-band edge at that point). As k_{\parallel} varies the miniband and minigap widths will also vary. In the case of symmetric (n, n) superlattices the adjacent minibands joined by zero energy gaps are slightly displaced horizontally, to be distinguishable.

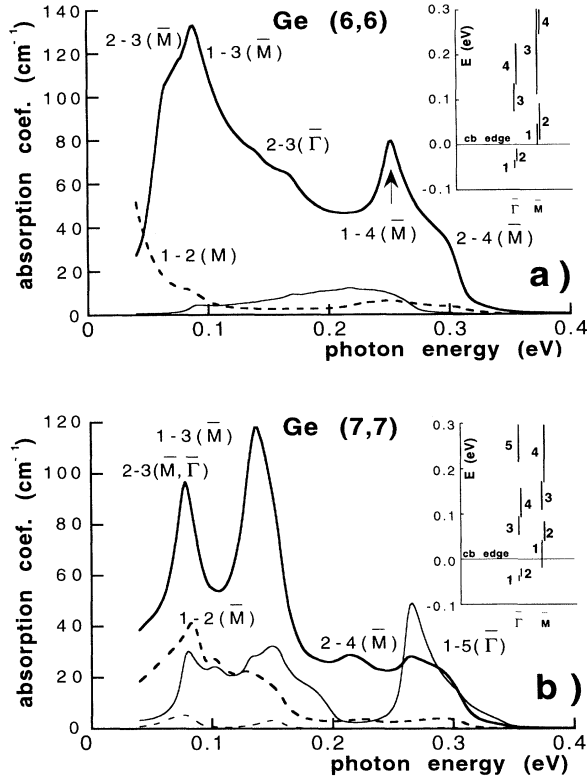


FIG. 2. Same as Fig. 1, but for Ge-based twinning superlattices: (a) Ge(6,6) and (b) Ge(7,7). The miniband structure in the insets is given at both the $\bar{\Gamma}$ and \bar{M} points.

show a rather sharp increase in absorption at very low photon energies. This arises due to transitions from states close to the lowest miniband top to those close to the next lowest miniband bottom. With a finite gap between the two minibands, this is exactly where one would expect significant mixing from the nearly free electron model, and hence comparatively large transition matrix elements. (Other $n \rightarrow n+1$ transitions, close to minigaps, would also contribute to low-energy absorption but do not since it is only the lowest miniband that is significantly populated.) The symmetric (n,n) superlattices, having zero energy gaps, lack this feature: states close to zero energy gaps do not interact strongly enough to give larger matrix elements, and states close to finite minigaps are too high in energy and therefore unpopulated, to given any amount of low-energy absorption. In the case of Ge-based twinning superlattices minibands at both $\bar{\Gamma}$ and \bar{M} points are important, because their energies are in the same range. Yet, Figs. 2(a) and 2(b) reveal that states at the \bar{M} point account for most of their optical activity. Actually, states at the $\bar{\Gamma}$ point are rather purely bulk L like, because valley mixing is not prominent at this point, and the fact that the $\bar{\Gamma}$ valley is not too remote from L does not help. At the \bar{M} point, however, valley mixing is very strong (enhanced by a small separation between the L and X valleys in Ge), which is reflected not only in peculiar miniband dispersion,¹⁰ but

in rather high values of transition matrix elements as well (especially close to miniband extrema). Typical largest values of the transition matrix elements ($|p_{if}|^2/m_0$) are of the order of 10^{-2} eV in Si-based superlattices, a few times 10^{-3} eV at the $\bar{\Gamma}$ point in Ge, and approximately 0.3 eV at the \bar{M} point in Ge.

One may also see from Figs. 1(a)–1(d) considering the more simple case of Si-based superlattices first, that increasing the temperature tends to smooth any local sharp features that might exist because of favorable matrix-element–density-of-states combinations. This is obviously due to smearing of the available electron distribution, but the overall, averaged absorption is actually somewhat enhanced. This latter effect may again be attributed to the fact that the increase of temperature (while still moderate so that upper minibands remain almost empty) tends to populate higher states of the first miniband, i.e., states closer to its top and the miniband gap, and therefore more active optically. The case of Ge superlattices is even more interesting. Changing the temperature here effectively transforms the superlattice from a quasi-direct-band-gap one into one that is more like the indirect-gap one (in the above-mentioned sense that majority of the electron population resides in minibands at the $\bar{\Gamma}$ or \bar{M} point). Since the two groups of minibands have very different optical properties, this results in a large dependence of the absorption in Ge-based twinning superlattices on temperature.

In the valence band we also find the miniband structure, examples of which are given in Figs. 3(a) and 3(b).

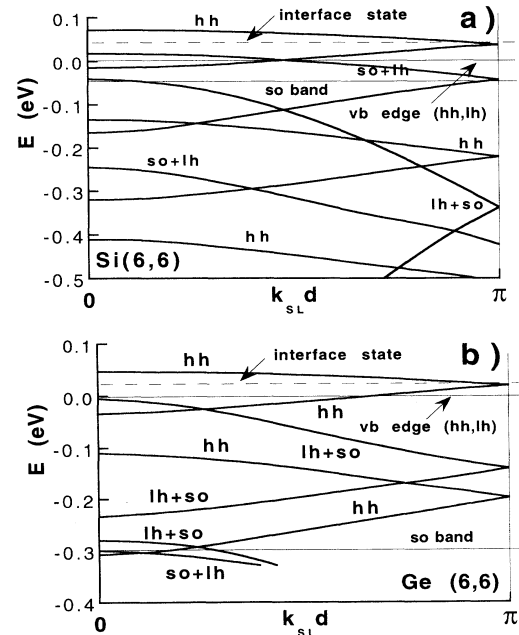


FIG. 3. The miniband dispersion in the valence band of (a) Si(6,6) and (b) Ge(6,6) twinning superlattices at the $\bar{\Gamma}$ point. The character of various branches is also denoted. Away from the exact $\bar{\Gamma}$ point anticrossings with finite gaps replace crossings.

The topmost miniband, which is heavy-hole-like, originates from the interface bound state (positioned above the valence-band top), and others are propagating state minibands, similar to those existing in conventional superlattices. While the wave functions of heavy-hole (hh) minibands have rather pure heavy-hole character, light-hole (lh) and split-off minibands have somewhat mixed character (especially in Si) even at the exact $\bar{\Gamma}$ point, though one of the states (lh or so) predominates. Off the $\bar{\Gamma}$ point state mixing is much more prominent, and instead of the miniband crossings seen in Figs. 3(a) and 3(b) one has anticrossing with finite gaps in between, as in conventional superlattices. Furthermore, instead of zero energy gaps at $\bar{\Gamma}$, finite gaps open for finite k_{\parallel} , measuring fractions of meV to a few meV, depending on the miniband pair and value of k_{\parallel} . As the superlattice period increases, the lowest pair of minibands would become increasingly narrow, and finally collapse into the interface bound state, which is 45 meV above the valence-band top in Si, and 27 meV in Ge (in the case of GaAs it amounts to 19 meV). For comparison, we note that the value we obtained for Si is between 19 and 100 meV predicted by the self-consistent calculations of Refs. 13 and 14, respectively.

In Figs. 4(a) and 4(b), we give the absorption arising from inter-valence-subband transitions in p -doped Si(6,6) and Ge(6,6) superlattices. The hole density is taken to be $p = 10^{17} \text{ cm}^{-3}$, where only the topmost pair of minibands

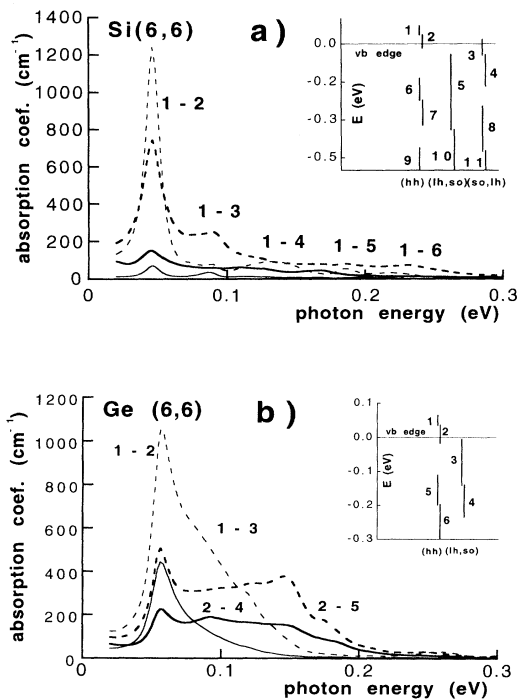


FIG. 4. The absorption coefficient arising from intersubband transitions within the valence band in (a)Si(6,6) and (b)Ge(6,6) twinning superlattices. The hole density is $p = 10^{17} \text{ cm}^{-3}$. The notation is the same as in Fig. 1, except that the miniband energies in the inset are measured from the valence-band top.

happens to be significantly populated (even at $T = 300 \text{ K}$). Considerably larger values of the absorption coefficient, in about the same range of photon energies, are found than in the case of conduction-band transitions. This is a consequence of the fact that hole states are more intensively scattered/mixed at twinning interfaces (note the larger gaps between minibands than is the case for the conduction band), and mixing is more prominent because of two or three degenerate or nearly degenerate hole states present, which all results in larger transition matrix elements. Unlike the case of conduction intersubband transitions, those in the valence band provide values of absorption that are comparable to what one has in conventional quantum wells (e.g., Ref. 19), and are thus of possible technical importance.

In any case, technically significant or not, the intersubband transitions in both the conduction and valence bands should be experimentally observable, because the absorption they provide significantly exceeds the values of free-carrier absorption in bulk (in various IV and III-V semiconductors with the doping density as used here and the same range of photon energies, p -doped samples have the absorption coefficient of the order 10^2 cm^{-1} , and n -doped of the order 5 cm^{-1} , e.g., Ref. 20).

B. Interband transitions

It has been established that folding effects may give rise to direct (phononless) interband optical transitions in superlattices made of indirect-gap materials, e.g., Si/GeSi. It is interesting to explore this feature in Ge-based twinning superlattices, where L points projected onto $\bar{\Gamma}$ may fold so that minibands they generate become direct in the superlattice Brillouin zone, and direct transitions between the valence-band minibands and L -derived minibands become allowed. Preliminary work on interband transitions in Ge twinning superlattices has been presented recently.²¹ The calculated interband absorption in the Ge(6,6) superlattice is given in Fig. 5(a). Values of the absorption coefficient are not large when compared to those in direct-band-gap materials like GaAs, but are still an order of magnitude higher than indirect, phonon-assisted absorption in bulk Ge at $T = 77\text{--}300 \text{ K}$ (e.g., Ref. 22) (however, no attempt was made here to optimize the twinning superlattice in this respect, and it may be that some $m \neq n$ case would offer somewhat larger absorption). For comparison, we note that in quasidirect Si/GeSi superlattices similar values of direct interband absorption have been found.²³

In accordance with the previous discussion, one may see that folding alone cannot provide direct absorption in indirect-gap semiconductors. The important issue is again the deviation of superlattice wave functions from folded bulk wave functions. Finite values of transition matrix elements in folded direct- (quasi-direct-) gap superlattices are really brought about by states mixing, i.e., modulation of bulk wave functions that make up the superlattice wave function (including the appearance of evanescent states), and these effects are usually not strong enough to make a quasi-direct-gap superlattice behave like a truly direct-gap superlattice or bulk. Looking in

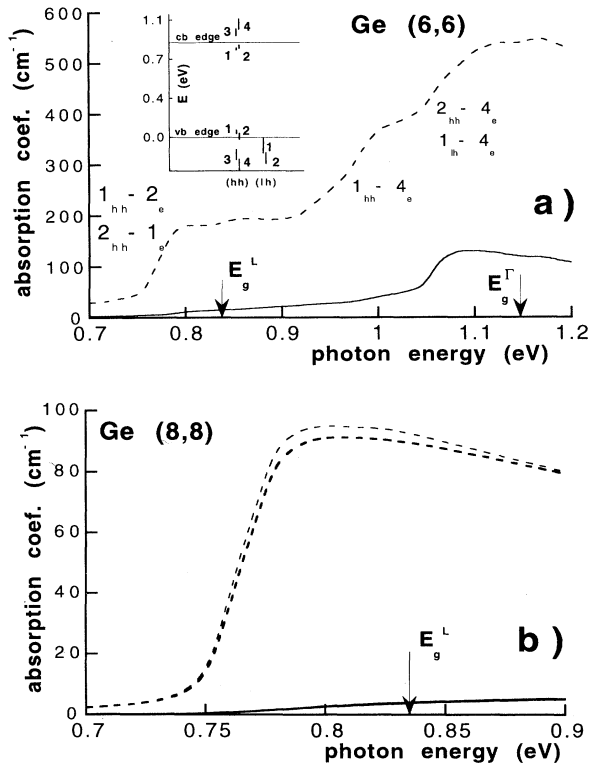


FIG. 5. The absorption due to interband direct transitions in (a)Ge(6,6) and (b)Ge(8,8) twinning superlattices. The notation in (a) is the same as in Fig. 1, except that there is no temperature dependence now. In (b) thick lines display the exact calculation, and thin lines show the results obtained within the axial approximation.

the structure of absorption in Fig. 5(a), one can see that there are two types of transitions that are really important. Those between the lowest pairs of minibands in both the conduction and valence bands have significant values of matrix elements because they are both interface-related minibands and thus have a good overlap (the bulk wave functions make the lowest conduction miniband, although purely L in character, are evanescent, modulated states, and thus escape the strict k -conservation rule). Also important are transitions between the lowest pair of hole minibands and the fourth conduction miniband. What gives rise to significant matrix elements here is the fact that this miniband is very close in energy to the Γ valley (which is approximately 0.3 eV above the L valley), so Γ - L mixing now becomes significant,¹⁰ and it is actually this small Γ contribution to the superlattice wave function that makes this miniband optically active. In either case the largest values of the transition matrix elements ($|p_{if}|^2/m_0$) are of the order 10^{-3} eV, well below those found in direct-gap semiconductors.

In Fig. 5(b) we give the absorption due only to evanescent state minibands in the Ge(8,8) superlattice, in a limited range of photon energies. Along with the results obtained as described in the previous section, results of the

axial approximation are also given for comparison. These are obtained by using the approximation that the miniband dispersion around the $\bar{\Gamma}$ point has a circular symmetry (while in fact it has a sixfold axial symmetry), and thus the k_{\parallel} points are sampled along a single line only (specifically, along the $\bar{\Gamma}$ - \bar{M} line). Obviously, the axial approximation works fine if only the $\bar{\Gamma}$ states are important, which is the case for valence intersubband transitions, and direct interband transitions, just as it does in ordinary (111) grown superlattices, e.g., GaAs/AlAs-based ones. We note that these transitions exist in Si-based superlattices as well, but there is no point in calculating them because the L valley in Si is 1 eV above X , so the folded direct transitions here would be completely screened by the phonon-assisted indirect absorption.

Finally, we give results for interband transitions in the GaAs(8,8) twinning superlattice, calculated within the axial approximation. Due to a very low scattering experienced by Γ electrons at the twinning boundary,¹⁰ the lowest conduction miniband has a dispersion that is almost identical to the folded bulk dispersion, its bottom being only slightly elevated from the conduction-band edge in bulk GaAs. In the valence band, however, there is a heavy-hole-like bound state at the twinning interface, and it generates the topmost pair of narrow hole minibands in the superlattice. Extrema of both minibands occur at the center of the superlattice Brillouin zone, and this is a direct-gap superlattice. In Fig. 6 we give the absorption arising from interband transitions between these evanescent hole minibands and the broad conduction miniband, a rather narrow range of photon energies where only these states give a contribution. The absorption coefficient here is quite large, as indeed is expected because these are truly direct transitions, allowed in bulk as well. The absorption threshold is somewhat redshifted, since the valence miniband is pushed above the bulk valence-band top more than is the conduction miniband bottom shifted above the bulk conduction-band bottom. However, for photon energies exceeding the band gap the absorption is lower than in bulk, since the transition matrix elements reach at most one-half of their bulk values, apparently due to the reduced overlap of piecewise-evanescent-like wave functions in the valence minibands

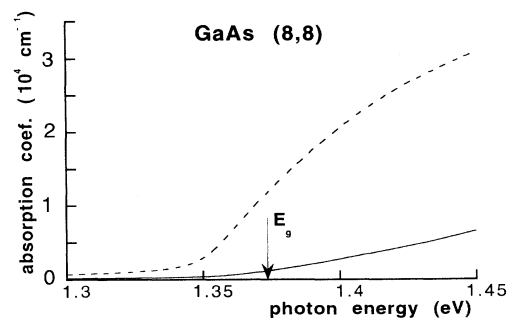


FIG. 6. The absorption coefficient close to threshold in the GaAs(8,8) superlattice. The notation is the same as in Fig. 5.

and propagatinglike wave functions in the conduction miniband. While there are a number of effects that induce the absorption profile, even in bulk, to deviate from the simplified theoretical predictions, it should still be possible to detect twinning in GaAs by polarization-sensitive measurements.

IV. CONCLUSION

The optical properties due to direct intersubband and interband transitions in the recently proposed twinning superlattices based on Si, Ge, and GaAs, were analyzed within the empirical pseudopotential framework. The

conduction-band intersubband absorption is found to be rather weak, but the absorption between the valence-band states may have rather high, possibly technically significant values. Direct (phononless) interband absorption in twinning superlattices based on indirect-gap semiconductors like Ge is also found to be possible.

ACKNOWLEDGMENTS

The authors would like to thank the EPSRC (UK) for computational facilities through the CSI scheme. One of the authors (Z.I.) is grateful to EPSRC (UK) for financial support.

-
- ¹Z. Ikonc, G. P. Srivastava, and J. C. Inkson, *Solid State Commun.* **86**, 799 (1993).
²S. Y. Ren and J. D. Dow, *Phys. Rev. B* **39**, 7796 (1989).
³M. Murayama and T. Nakayama, *J. Phys. Soc. Jpn.* **61**, 2419 (1992).
⁴J. P. Stark, *Phys. Rev. B* **38**, 1139 (1988).
⁵R. L. Headrick, B. E. Weir, J. Bevk, B. S. Freer, D. J. Eaglesham, and L. C. Feldman, *Phys. Rev. Lett.* **65**, 1128 (1990).
⁶M. Koguchi, H. Kakibayashi, M. Yazawa, K. Hiruma, and T. Katsuyama, *Jpn. J. Appl. Phys.* **31**, 2061 (1992).
⁷K. Hiruma *et al.*, *J. Appl. Phys.* **74**, 3162 (1993).
⁸M. Fujii, H. Iwanaga, and N. Shibata, *J. Cryst. Growth* **91**, 229 (1988).
⁹P. Becla, A. F. Witt, and C. F. Dewey, Jr., *J. Vac. Sci. Technol. B* **10**, 1594 (1992).
¹⁰Z. Ikonc, G. P. Srivastava, and J. C. Inkson, *Phys. Rev. B* **48**, 17 181 (1993).
¹¹D. Y. K. Ko and J. C. Inkson, *Phys. Rev. B* **38**, 9945 (1988).
¹²Z. Ikonc, G. P. Srivastava, and J. C. Inkson, *Phys. Rev. B* **46**, 15 150 (1992).
¹³M. D. Stiles and D. R. Hamann, *Phys. Rev. B* **38**, 2021 (1988).
¹⁴M. Y. Chou, M. L. Cohen, and S. G. Louie, *Phys. Rev. B* **32**, 7979 (1985).
¹⁵J. R. Chelikowsky and M. L. Cohen, *Phys. Rev. B* **14**, 556 (1976).
¹⁶M. L. Cohen and T. K. Bergstresser, *Phys. Rev.* **141**, 789 (1966).
¹⁷E. Caruthers and C.-L. Chung, *Phys. Rev. B* **17**, 2705 (1978).
¹⁸Y. Zhang, N. Baruch, and W. I. Wang, *J. Appl. Phys.* **75**, 3690 (1994).
¹⁹P. Man and D. S. Pan, *Appl. Phys. Lett.* **61**, 2799 (1992).
²⁰H. Y. Fan, in *Semiconductors and Semimetals*, edited by R. K. Willardson and A. C. Beer (Academic, New York, 1967), Vol. 3, pp. 409–414.
²¹Z. Ikonc, G. P. Srivastava, and J. C. Inkson, *Phys. Rev. B* **52**, 1474 (1995).
²²B. K. Ridley, *Quantum Processes in Semiconductors* (Clarendon, Oxford, 1993), pp. 218–220.
²³C. Tserbak and G. Theodorou, *Phys. Rev. B* **50**, 18 179 (1994).